Nanotechnology **20** (2009) 215608 (7pp) doi:10.1088/0957-4484/20/21/215608

A three-dimensional, biaxially textured oxide nanofence composed of MgO single crystal nanobelt segments

Sung Hun Wee[1,2], Amit Goyal[1], Karren L More[1] and Eliot Specht[1]

[1] Materials Science and Technology Division, Oak Ridge National Laboratory, Oak Ridge, TN 37831, USA
[2] Department of Materials Science and Engineering, University of Tennessee, Knoxville, TN 37996, USA

E-mail: goyala@ornl.gov

Received 28 January 2009, in final form 19 March 2009
Published 6 May 2009
Online at stacks.iop.org/Nano/20/215608

Abstract
A unique, three-dimensional (3D), biaxially textured, MgO, nanofence comprised of single crystal MgO nanobelt segments or links was synthesized via epitaxial growth on (100) $SrTiO_3$ substrates. Individual single crystal MgO nanobelt segments comprising the nanofence have a square cross-section with dimensions in the range of 10–20 nm and with lengths in the range from 100 nm up to 1 μm. X-ray diffraction shows that the 3D MgO nanofence has an epitaxial relation with (100) $SrTiO_3$ substrates with a cube-on-cube, $\{100\}\langle 100\rangle$ orientation and with values of the full width at half-maximum of the (200) ω-scan and the (110) φ-scan at 4.5° and 5.5°, respectively. Such a biaxially textured oxide nanofence with single crystal segments can be used as a 3D nanotemplated substrate for epitaxial growth of wide-ranging, 3D, electronic, magnetic and electromagnetic nanodevices.

(Some figures in this article are in colour only in the electronic version)

One-dimensional (1D) nanostructures such as nanowires, nanotubes, and nanobelts have attracted significant research attention world-wide because of their potential use in electrical, magnetic and electromagnetic nanodevices. Such nanoscale devices are also expected to exhibit unique physical properties due to low dimensionality. Novel nanodevices constructed from individual 1D nanostructures of semiconductors, metals, and oxides have been studied [1, 2]. In a 'bottom-up' approach to fabrication of nanoscale devices, nanowires or nanobelts are viewed as nanoscale building blocks which can be used to assemble integrated nanoscale devices. However, typical nanowire or nanobelt synthesis results in bundles of randomly oriented nanowires which are physically entangled [3–6, 13]. Assembling the wires or belts from the entangled bundles requires time-consuming, complex, and expensive steps to form the devices [7, 8]. In order to avoid these steps, it is crucial to grow nanowires or nanobelts in self-assembled architectures which can result in controlled and reproducible fabrication. Synthesis of polycrystalline, two-dimensional (2D) nanowire arrays has been achieved via selectively patterned metal catalyst templates via lithography as well as by growth on pre-formed nanopores templates made by anodizing aluminum oxide [9–11]. There are no reports of synthesis of 2D nanowire or nanobelts arrays *without* the use of an expensive and/or complicated templating process such as lithography. There are also no reports of controlled and reproducible synthesis of a polycrystalline, 3D nanowire or nanobelt array with or without the use of a nanostructured template. Lastly, there are no reports of three-dimensional (3D), self-assembled, epitaxial oxide fences comprised of single crystal nanobelts. Such 3D, single crystal, nanofences can serve as nanotemplates for epitaxial growth of a whole range of novel nanodevices.

In this paper, we report on fabrication of epitaxial, self-assembled, 3D nanofences via a simple and novel approach which can easily be scaled-up and potentially be used to fabricate similar structures of a number of compounds. The technique utilizes co-laser ablation of a source material and a metal catalyst that assists nanowire growth via vapor–liquid–solid (VLS) mechanism. The material chosen to demonstrate

 © 2009 IOP Publishing Ltd Printed in the UK

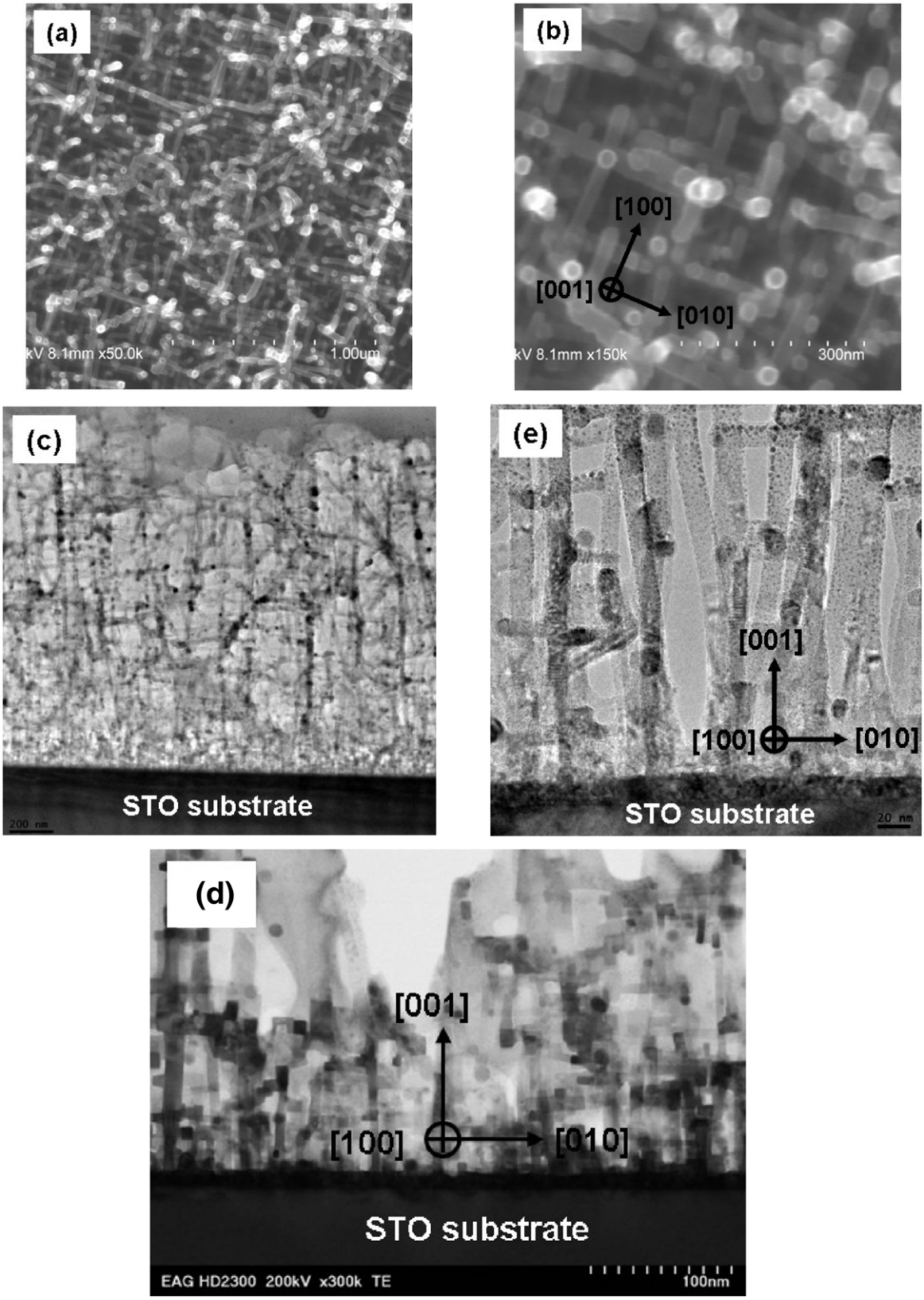

Figure 1. Morphology for 3D, biaxially textured, MgO nanofence epitaxially grown on (100) $SrTiO_3$ substrate. (a) and (b), Top-view, FE-SEM images showing MgO nanofence at low (a) and high (b) magnification. The higher magnification SEM image shows the 3D nanofence structure clearly. (c) Cross-section TEM image of MgO nanobelts at a low magnification showing that individual vertical nanobelts comprising the nanofence can be up to 1 μm long. (d) Higher magnification cross-section image near the STO substrate clearly showing the ⟨100⟩ oriented MgO nanofence w.r.t. the STO substrate. (e) Higher magnification TEM image of the nanofence. The small dots on the surface of MgO nanobelts are platinum particles coming from TEM specimen preparation (a thin layer of Pt was sputtered on the surface before fabrication of sample via the focused-ion-beam (FIB) approach).

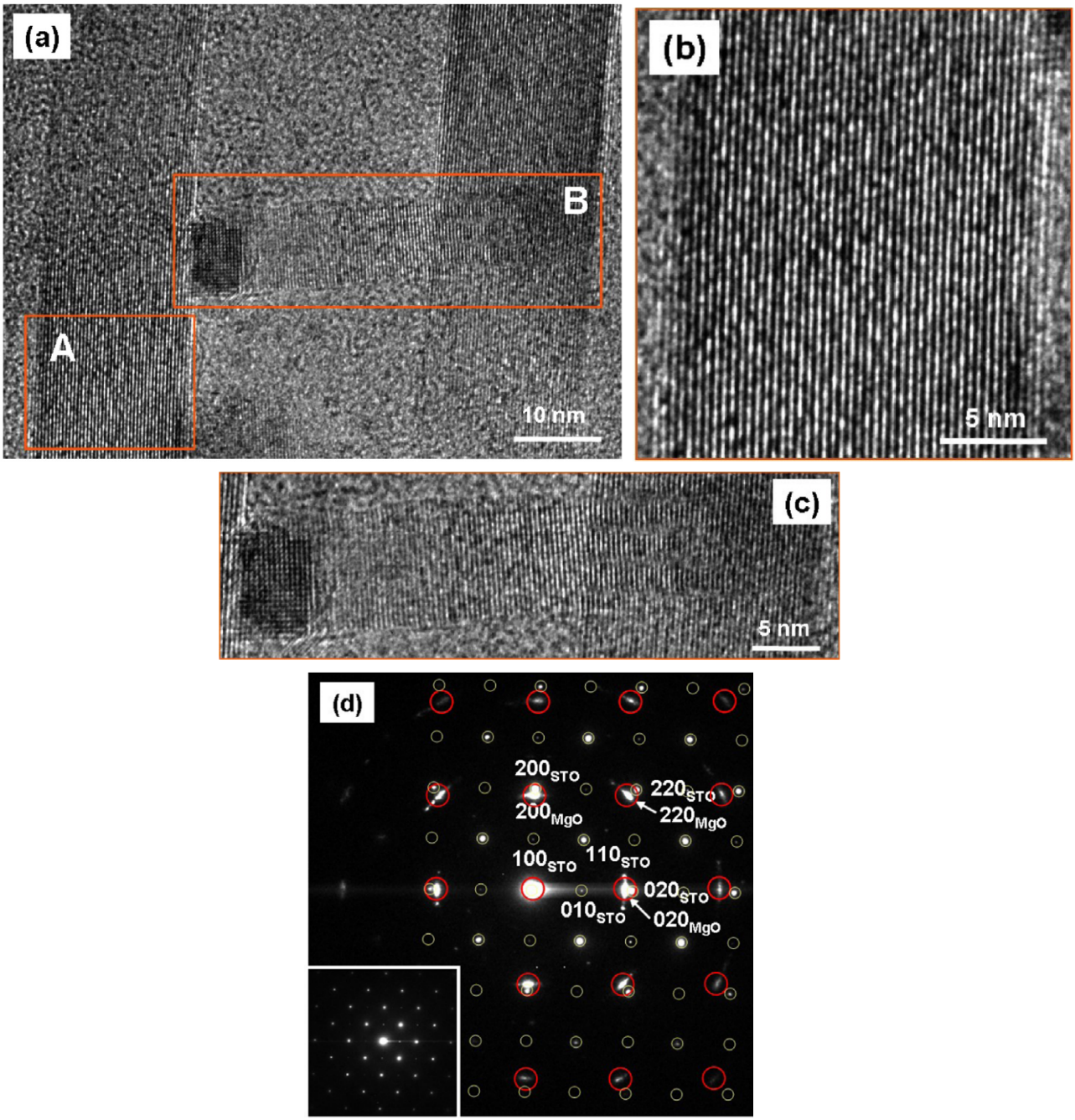

Figure 2. High resolution TEM analysis for MgO nanobelts. (a) High resolution TEM image showing clear lattice fringes in MgO nanobelts. (b) Higher magnification image of section 'A' showing that the lattice fringes continue to the edge of the nanobelt. (c) Higher magnification image of horizontal link 'B' showing that the lattice fringes continue to the edge of this nanobelt. (d) SAD pattern obtained from the MgO nanofence and the STO substrate. Red and yellow circles indicate diffraction spots coming from the MgO nanobelts and STO substrate, respectively. Inset of (d) shows SAD pattern for STO substrate.

fabrication of 3D epitaxial, oxide nanofence in this study is magnesium oxide (MgO). This is a typical binary oxide and MgO nanowires have already been synthesized using a metal catalyst such as gold [6, 10, 12]. MgO is also widely used as a template to fabricate epitaxial films of many oxides having multiple functionalities that include semiconducting, ferroelectric, ferromagnetic, and superconducting properties, due to its structural similarity and low lattice mismatch with these materials.

3D self-assembled MgO nanobelts were epitaxially grown on (100) $SrTiO_3$ (STO) substrate via co-laser ablation of MgO and Ni catalyst using KrF excimer laser ($\lambda = 248$ nm) at a repetition rate of 10 Hz. To accomplish co-deposition, a 3 mm wide Ni metal foil was attached to the surface of MgO target. When the target was rotated, one shot of Ni was periodically ablated per 10–11 shots for MgO. Laser energy density and substrate to target distance was set to 4 J cm^{-2} and 7 cm, respectively. A substrate temperature (T_s) of 780 °C

and a deposition pressure of 200 mTorr, 4%H_2/Ar gas was used. After deposition, samples were cooled down to room temperature at a cooling rate of 20 °C min^{-1}. Phase and texture analysis was performed using a Picker 4-circle diffractometer with Cu Kα radiation for θ–2θ, ω and φ-scans, respectively. Microstructures for samples were characterized via field emission scanning electron microscopy (Hitachi S4800 FE-SEM) and transmission electron microscopy (Hitachi HF-3300 TEM).

Continuous supply of the catalyst, Ni metal, during growth was key to the synthesis of 3D, biaxially textured MgO nanofence with a unique, self-organized structure along ⟨100⟩ directions of (100) STO substrate. Figure 1 shows plane-view FE-SEM and cross-section TEM images for the MgO nanofence grown epitaxially on the (100) STO substrate. This particular sample was grown using a standard MgO target with a Ni strip attached to it and covering ∼9% area of the target. Since the laser plume for ablation from Ni was almost half size that for MgO, the actual quantity of Ni in the sample is expected to be much less than 9%. As shown in figures 1(a) and (b), FE-SEM images show semi-transparent MgO nanobelts that grow horizontally, parallel to the surface of STO substrate. The nanobelts are observed to have high aspect ratios with uniform diameters of 10–20 nm and lengths of 100–300 nm. It can be also seen that the nanobelts are not randomly distributed but aligned along [100] and [010] directions of the STO(100) substrate, as denoted by arrows in figure 1(b). Such a self-assembled pattern of MgO nanobelts resembles a 3D 'fence'. Since the SEM images were obtained from the top of the sample, nanobelts that grow perpendicular to STO substrate are not easily observed. Only Ni catalyst-based nanospheres, imaged brightly in the SEM image, at tips of these vertical nanobelts of square cross-section are clearly visible. The vertically grown nanobelts were also examined using cross-sectional TEM microscopy as shown in figures 1(c)–(e). The large, darkly imaging spheres shown in the figures are the Ni catalyst. In figure 1(e), visible small dots on semi-transparent nanobelts were identified as platinum particles used for focused-ion-beam (FIB) preparation of TEM specimens. Once the contamination of a TEM specimen via platinum particles had been identified, another TEM specimen with no platinum particles decoration was carefully prepared using a special procedure. TEM images of figures 1(c) and (d) and figure 2(a) were obtained from the latter TEM specimen. Figure 1(c) shows entire cross-section of the sample showing that vertical nanobelts have much higher aspect ratios with square cross-section, 10–20 nm on a side and with long lengths from 100 nm up to 1 μm, than those that grow horizontally. As shown in figures 1(d) and (e), another interesting feature is that all horizontally grown nanobelts oriented along the [100] and [010] directions of STO are stemming from the nanobelts that grow vertically in general along STO[001] direction. One can also see that some of these ∼90° branched nanobelts connect vertically grown nanobelts like a 'sky bridge' between two skyscrapers.

Further TEM study was performed to examine individual MgO nanobelts more closely, as shown in figure 2. Figure 2(a) shows a high resolution TEM image showing lattice fringes in MgO nanobelts indicating their single crystalline nature as evidenced by the visible lattice fringes. Figure 2(b) shows a higher magnification image of the region shown marked 'A' in figure 2(a). It can clearly be seen that the MgO lattice fringes extend all the way to the edges of the nanobelt. This single crystal nature of individual segments comprising the nanofence is essential for subsequent growth of epitaxial, nanodevices. Figure 2(c) shows a higher magnification image of horizontal link connecting the two vertical nanobelts shown in figure 2(a).

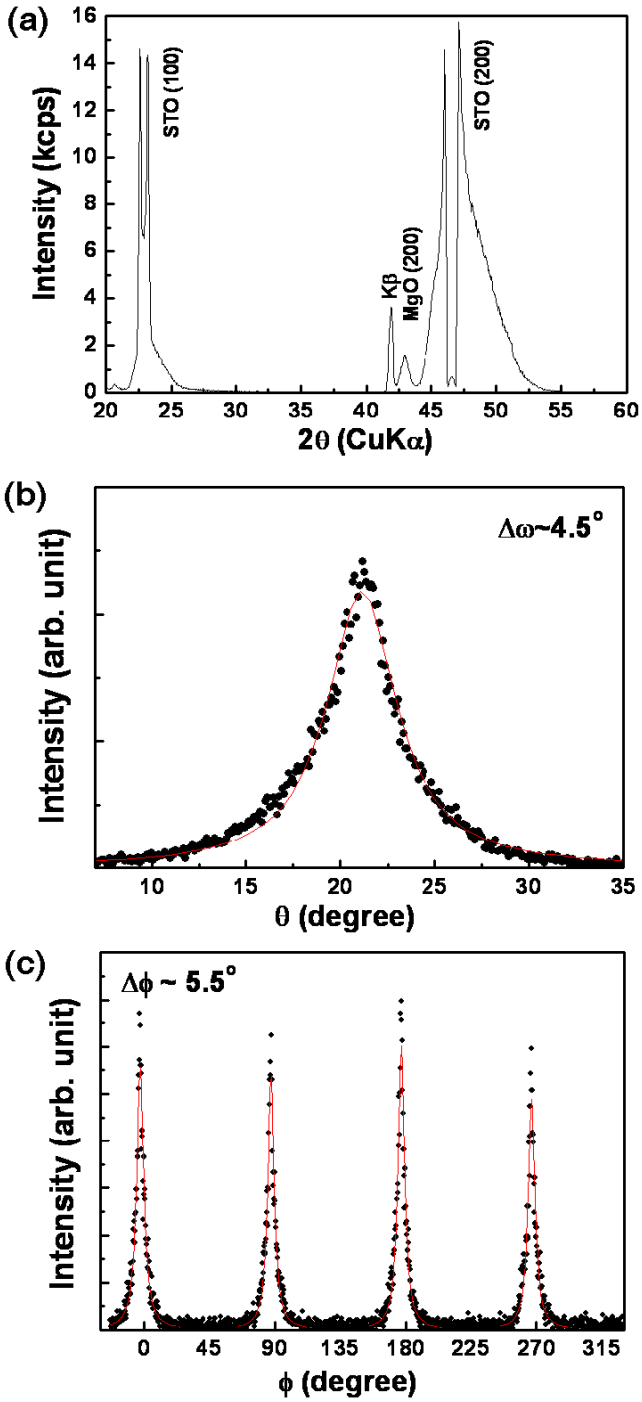

Figure 3. XRD diffraction results obtained from entire MgO 'nanofence' layer. (a) θ–2θ scan, (b) (200) ω-scan, and (c) (220) φ-scan.

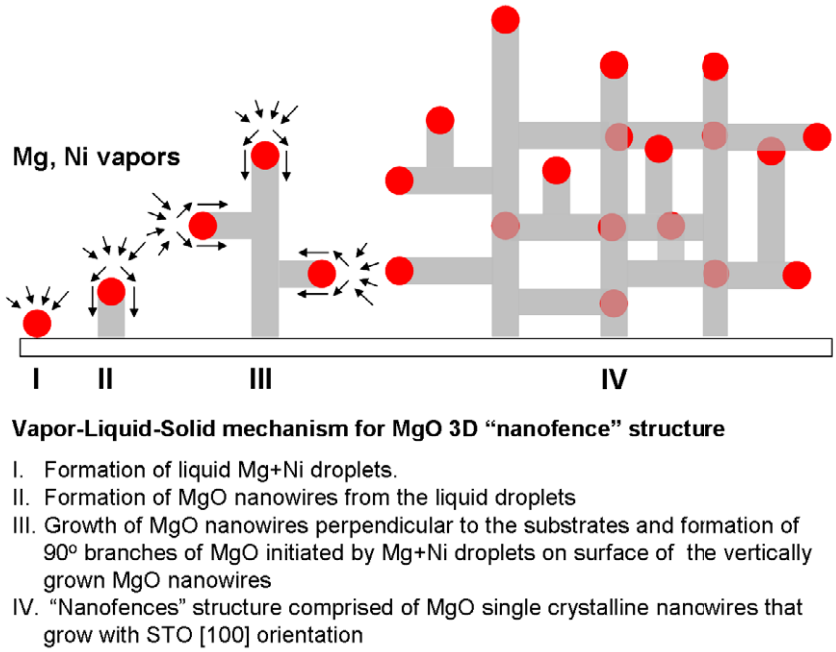

Figure 4. Schematic diagram for growth of MgO 'nanofence' structure via VLS mechanism.

Two points are obvious from the image. The first is the slight tilt of the horizontal link from the ⟨100⟩ directions of STO. Such deviations result in the observed overall FWHM of omega and phi scans in the range of 4.4°–5.5°. The second is that the horizontal link, while tilted slightly from ⟨100⟩ directions, is also fully single crystalline. This is again clear from the lattice fringes of the link. Please note that at either ends, Moiré fringes due to two intersecting lattices from the vertical and horizontal nanobelts are observed. Figure 2(d) shows a selected diffraction pattern (SAD) obtained from a region including the 3D MgO nanofence and the STO substrate. Diffraction spots for MgO single crystalline nanobelts (denoted by red circles) are slightly overlapped with but distinguishable from those for STO substrate (denoted by yellow circles) also shown in the inset of the figure, due to the difference in their lattice parameters ($a_{MgO} = 4.21$ Å and $a_{STO} = 3.905$ Å). This result indicates epitaxial relationship between MgO nanobelts and STO substrate with $[100]_{MgO} \parallel [100]_{STO}$.

Figure 3 shows bulk x-ray diffraction (XRD) results obtained from entire 3D MgO nanofence layer. The θ–2θ scan shows only single MgO(200) peak with (h00) peaks of STO substrate. No peaks related to extra MgO crystallographic orientations are detected from a wide range of the scan. In-plane and out-of-plane textures for the sample are also determined by (200) ω- and (220) φ-scans. The full width at half-maximum, FWHM, of the (200) ω-scan and (220) φ-scan were measured to be ∼4.5° and ∼5.5°, respectively which are relatively broader than the values ($\Delta\omega \sim 1.0$, $\Delta\varphi \sim 1.2$) for reference sample, epitaxial MgO film grown on STO substrate. The XRD results for the sample are completely consistent with what we observed from the SEM and TEM images shown in figures 1 and 2. If MgO nanobelts were randomly distributed, multiple orientations for MgO phase would be detected from θ–2θ scan for the sample, like previously reported results [6, 13]. The peak broadening of the MgO(200), 2θ peak is due to the nanoscale size of the MgO nanobelts. Large FWHM values in the ω- and φ-scans arise from the misalignments for MgO nanobelts which grow with vertical and horizontal directions, respectively with respect to STO substrate as shown in the SEM and TEM images of figures 1 and 2.

A schematic diagram to explain the formation of such a 3D nanofence structure is illustrated in figure 4. As expected, the VLS mechanism is responsible for the formation of this structure. As shown figures 1 and 2, Ni-based nanocluster spheres are clearly observed at the tips of nearly all of the nanobelts, which is a key evidence for the VLS mechanism [1–3, 10, 12]. Note that these Ni-based spheres can be easily removed if necessary, using proper etching agents such as $HCl:HNO_3 = 5:1$ and $HF:HNO_3 = 1:1$. (This may be required for subsequent growth of epitaxial nanoscale devices.) In the schematic of the growth process resulting in the 3D nanofence structure, at the first stage (I), Mg and Ni vapors ablated from the target condense and form nanoscale Mg–Ni liquid droplets on the surface of the substrate. Although pure Ni has high melting point (m.p. = 1450 °C), binary phase diagram of Mg–Ni shows that Mg-rich, Mg–Ni nanoclusters can exist as liquid phase at the growth temperature of ∼780 °C. Similarly, Au catalyst, one of widely used catalysts for growth of MgO nanowires [6, 10, 12], also has the m.p. of ∼1080 °C but Mg–Au clusters can exist in liquid phase at much lower temperature than the m.p. of Au. In the second stage (II), excess Mg in the liquid droplets reacts with oxygen atoms or molecules, and forms solid MgO nanobelts that continue to grow vertically. Since a forming gas of 4%H_2/Ar was used for the growth to avoid oxidation of Ni catalyst, very limited quantity of oxygen atoms or molecules was supplied from MgO target or residual oxygen molecules in chamber.

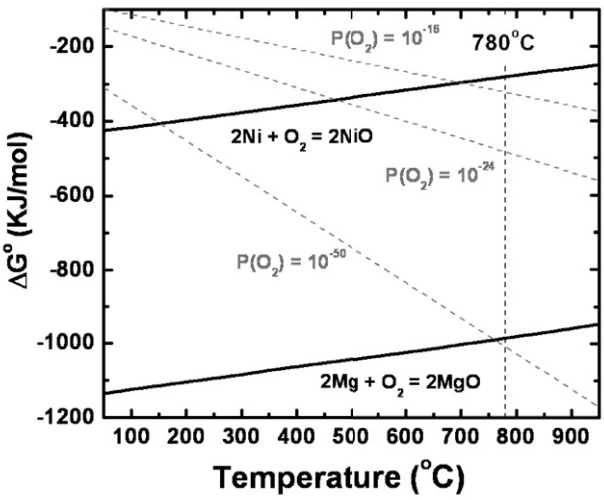

Figure 5. Ellingham diagram for Ni/NiO and Mg/MgO showing MgO and Ni with no oxidation are stable in the $P(O_2)$ range of 10^{-16}–10^{-24} atm at the temperature of 780 °C.

Oxygen partial pressure level in the chamber is expected to be in the range of 10^{-16}–10^{-24} atm, when deposition is performed at 200 mTorr of 4%H_2/Ar.[3] Figure 5 displays Ellingham diagram for Ni/NiO and Mg/MgO. At the growth temperature of 780 °C, these oxygen pressure levels thermodynamically allow stable MgO and Ni without oxidation, indicating that this oxygen quantity should be enough to form MgO nanobelts assisted by Ni catalyst. It is also noted that no difference in structural and morphological features were also found between the samples with and without *in situ* post-oxygen annealing at 500 °C for 30 min in $P(O_2) = 500$ Torr after deposition, implying that sufficient oxygen was available during growth. It is important to note that square cross-section nanobelts are observed as opposed to round diameter 'nanowires'. This occurs due to the highly anisotropic surface energies of ceramics such as MgO. The {100} planes are the lowest surface energy planes [14] and hence form the facets on these nanobelts. Since in cross-section of the vertical nanobelt, a similar growth rate is expected for the two different directions [100] or [010], a square cross-section results. Growth along the [100] direction is driven by the Ni catalyst. During the growth, in the third stage (III), Mg–Ni liquid droplets are also formed on the surface of vertically growing MgO nanobelts due to the continuous supply of Ni catalyst during growth. Hence MgO nanobelts nucleate and grow horizontally, parallel to the substrate as well. For one set of horizontally oriented nanobelts, the growth rate along the [010] and [001] is the same and the growth along [100] is driven by the Ni catalyst. For the other set of horizontally oriented nanobelts, the growth rate along the [100] and [001] is the same and the growth along [010] is driven by the Ni catalyst. Consequently, in the fourth stage (IV), the growth of single crystal, MgO nanobelts, both vertically and horizontally and aligned along STO⟨100⟩ directions results in a self-assembled, 3D nanofence structure shown in figures 1 and 2.

[3] It is difficult to estimate directly the accurate $P(O_2)$ levels in deposition pressure of 200 mTorr when using 4%H_2/Ar gas. Hence, the speculation of $P(O_2)$ levels is based on the measurement of $P(O_2)$ using zirconia oxygen sensor in quartz tube furnace where 4%H_2/Ar gas with and without small amount of water vapor flows at temperature ranges of 750–1150 °C, in atmospheric condition.

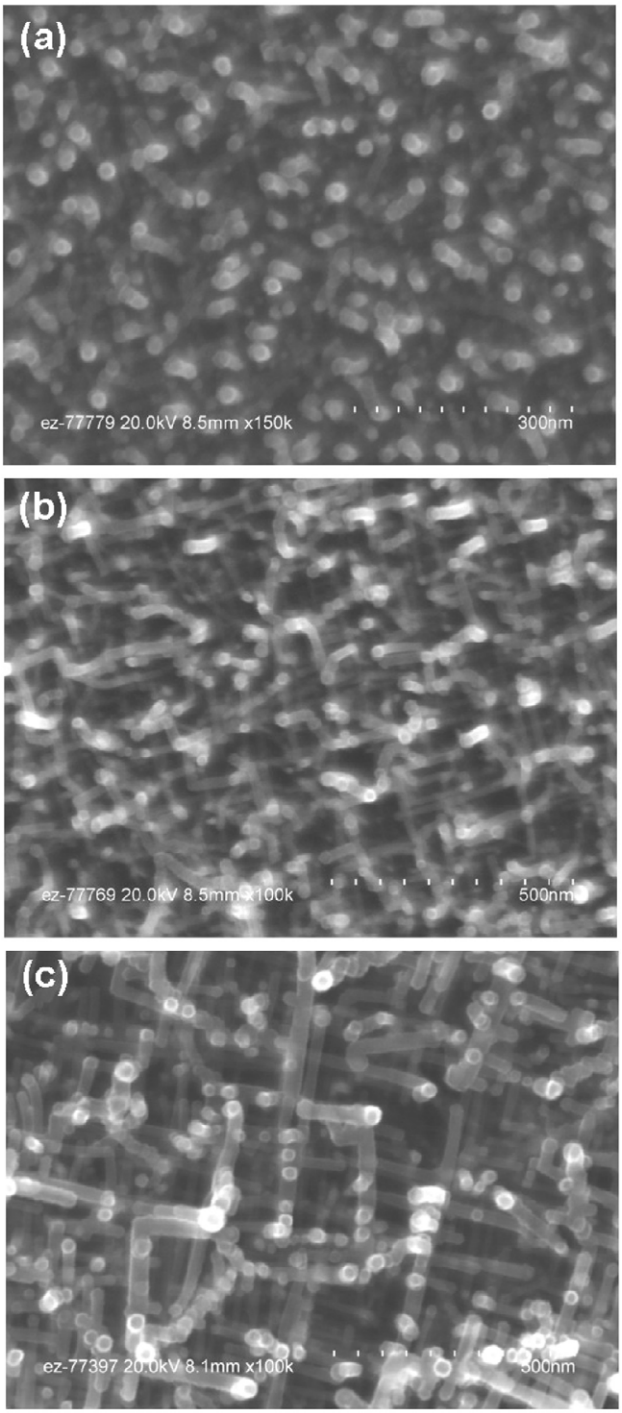

Figure 6. Plane-view, SEM images for MgO nanobelts for different growth times of (a) 5 min, (b) 10 min, and (c) 30 min. Note that magnifications are 150$k\times$ for (a) and 100$k\times$ for (b) and (c).

The formation process of 3D MgO nanofence schematically illustrated in figure 4 was also confirmed by plane-view SEM images taken from the samples grown for different growth times, as shown in figure 6. MgO nanobelts indeed

grow almost only in vertical direction when they start to grow (figure 6(a)). After initial growth of MgO nanobelts vertically, the horizontal growth of 90° branched, MgO nanobelts occurs on the surface of vertically grown MgO nanobelts by continuous supply of the Ni catalyst (figure 6(b)). Finally, the 3D nanofence comprised of self-assembled single crystalline, MgO nanobelt segments is formed as shown in figure 6(c). Similar 3D nanofences using the method described in this paper should be possible for a range of materials by an appropriate selection of the catalyst material. Lastly, since the 3D nanofence is completely heteroepitaxial, such structures can be produced reproducibly and on large area substrates. Any device stack that can be grown epitaxially on a flat, macroscopic, single crystal MgO substrate can now be grown on the 3D nanotemplated substrate.

In summary, a simple and controlled method to fabricate a 3D, epitaxial, biaxially textured nanofence comprised of single crystalline MgO nanobelt segments or links that grew both vertically and horizontally along ⟨100⟩ directions of the (100) STO substrate was developed. Continuous supply of Ni catalyst during the co-laser ablation of MgO and Ni metal led to the growth of nanobelts with such a unique morphology. Individual single crystalline MgO nanobelts had a square cross-section with high aspect ratios. X-ray diffraction results obtained from an entire MgO nanofence layer confirmed that MgO nanofence had epitaxial relation with STO substrate of $[100]_{MgO} \parallel [100]_{STO}$. Such oxide nanofences can be used as a 3D biaxially textured nanotemplate for epitaxial growth of wide-ranging, 3D, electronic, magnetic and electromagnetic nanodevices.

Acknowledgments

Authors would like to thank T Thundat and J S Shin at Oak Ridge National Laboratory for review of the paper. Research was sponsored by the Laboratory Directed Research and Development Program of Oak Ridge National Laboratory (ORNL), managed by UT-Battelle, LLC for the US Department of Energy. Research was supported in part by the Oak Ridge National Laboratory SHaRE User Facility, Division of Scientific User Facilities, Office of Basic Energy Science, US Department of Energy.

References

[1] Lu W and Lieber C M 2006 *J. Phys. D: Appl. Phys.* **39** R387
[2] Wang N, Cai Y and Zhang R Q 2008 *Mater. Sci. Eng.* R **60** 1
[3] Morales A M and Liber C M 1998 *Science* **279** 208
[4] Duan X, Huang Y, Cui Y and Wang J 2001 *Nature* **409** 66
[5] Pan Z W, Dai Z R and Wang Z L 2001 *Science* **291** 1947
[6] Kar S and Chaudhuri S 2006 *J. Nanosci. Nanotechnol.* **6** 1447
[7] Ahn J H *et al* 2006 *Science* **314** 1754
[8] Javey A, Nam S, Friedman R S, Yan H and Lieber C M 2007 *Nano Lett.* **7** 773
[9] Liang Y, Zhen C, Zou D and Xu D 2004 *J. Am. Chem. Soc.* **126** 16338
[10] Nagashima K, Yanagida T, Tanaka H and Kawai T 2007 *J. Appl. Phys.* **101** 12304
[11] Huang M H *et al* 2001 *Science* **8** 1897
[12] Han S *et al* 2004 *Nano Lett.* **4** 1241
[13] Hu L *et al* 2004 *J. Nanosci. Nanotechnol.* **4** 1071
[14] Saylor D M, Mason D E and Rohrer G S 2000 *J. Am. Ceram. Soc.* **83** 1226